Cent. Eur. J. Geosci. • 5(3) • 2013 • 354-373
DOI: 10.2478/s13533-012-0134-7

VERSITA

Central European Journal of **Geosciences**

New geological model of the Lagoa Real uraniferous albitites from Bahia (Brazil)

Research Article

Alexandre de Oliveira Chaves*

Institute of Geosciences - Minas Gerais Federal University (IGC-UFMG) - Brazil

Received 24 April 2013; accepted 8 July 2013

Abstract: New evidence supported by petrography (including mineral chemistry), lithogeochemistry, U-Pb geochronology by Laser Ablation Inductively Coupled Plasma Mass Spectrometry (LA-ICP-MS), and physicochemical study of fluid and melt inclusions by LA-ICP-MS and microthermometry, point to an orogenic setting of Lagoa Real (Bahia-Brazil) involving uraniferous mineralization . Unlike the previous models in which uraniferous albitites represent Na-metasomatised 1.75 Ga anorogenic granitic rocks, it is understood here that they correspond to metamorphosed sodium-rich and quartz-free 1.9 Ga late-orogenic syenitic rocks (Na-metasyenites). These syenitic rocks are rich not only in albite, but also in U-rich titanite (source of uranium). The interpretation of geochemical data points to a petrogenetic connection between alkali-diorite (local amphibolite protolith) and sodic syenite by fractional crystallization through a transalkaline series. This magmatic differentiation occurred either before or during shear processes, which in turn led to albitite and amphibolite formation. The metamorphic reactions, which include intense recrystallization of magmatic minerals, led uraninite to precipitate at 1.87 Ga under Oxidation/Reduction control. A second population of uraninites was also generated by the reactivation of shear zones during the 0.6 Ga Brasiliano Orogeny. The geotectonic implications include the importance of the Orosirian event in the Paramirim Block during paleoproterozoic São Francisco Craton edification and the influence of the Brasiliano event in the Paramirim Block during the West-Gondwana assembly processes. The regional microcline-gneiss, whose protolith is a 2.0 Ga syn-collisional potassic granite, represents the albitite host rock. The microcilne-gneiss has no petrogenetic association to the syenite (albitite protolith) in magmatic evolutionary terms.

Keywords: Lagoa Real • uraniferous albitites • late-orogenic syenite • LA-ICP-MS • U-Pb

1. Introduction

Currently, there is only one active uranium mine in Latin America located at Lagoa Real district, State of Bahia – Brazil (Figure 1), which is found in the central area of the São Francisco Craton. The Lagoa Real Uraniferous Province and its surroundings have been the subject of geological and aerogeophysical surveys [1–3] and of various studies of the origin and control of uranium deposits, including those of [4–12]. Some of these studies disagree about the age of the Lagoa Real uraniferous mineralization, but usually its genesis is attributed to uranium and sodium-bearing hydrothermal fluids, which metasomatised the 1.75 Ga anorogenic São Timóteo granite (granite age by [7, 10, 13]) to yield U-rich albitites.

[14] show? that many uranium rich provinces are related to evolved felsic igneous rocks intruded into the crust, not only anorogenically, but also during the final stages of

*E-mail: alex2010@ufmg.br

orogenesis. According to [15], during the late orogenic stages, ductile shear fault zones controlled the site of emplacement of felsic magmatic provinces. Pressure release caused by the faulting can produce a partial melting in the deep zones of the thickened orogenic lithosphere. Furthermore, the partial melting of the lithospheric mantle above the subducted slab is also supported by the dehydration of the latter. The interaction between fluids generated during this dehydration and overlaying mantle material would be responsible for the trace and rare earth elements, thorium, and uranium enrichment in magmas [16]. When submitted to fractional crystallization processes, such magmas eventually evolve to U-rich felsic lithotypes.

New evidence presented here, supported by petrography (including mineral chemistry), lithogeochemistry, LA-ICP-MS U-Pb geochronology, and physicochemical study of fluid and melt inclusions by LA-ICP-MS and microthermometry, show an orogenic setting older than 1.75 Ga involving uraniferous mineralization of Lagoa Real. This raises the question: are the uraniferous albitites Na-metasomatised granitic rocks or are they metamorphosed sodium-rich and quartz-free magmatic rocks (Na-metasyenites)?

Therefore, the aim of the present study is to propose a new geological model able to explain the relationship between magmatism, shearing, subsequent metamorphic reactions and U mineralization of Lagoa Real as well as the tectonic implications under a new scenario.

2. Geological setting of the Lagoa Real Uraniferous Province

The Lagoa Real region is located in the central-southern part of São Francisco Craton (Figure 1). The basement of this region is formed by Archean/Palaeoproterozoic granulitic, migmatitic, and gneissic rocks, which belong to the Paramirim and Gavião blocks [17]. The Ibitira-Brumado volcanosedimentary unit is found in the area and comprises amphibolites, banded iron formations, gneisses, metacherts, marbles, and schists. [18] interpreted this unit as a Lower Palaeoproterozoic greenstone belt. The Palaeoproterozoic Lagoa Real Granitic-Gneissic Complex covers an area larger than 2,000 km^2 of the Paramirim Block and includes granitoid bodies, gneisses, albitites and amphibolites. [8] attributed the genesis of the uranium-bearing albitites to metamorphism and progressive deformation of the 1.75 Ga anorogenic São Timóteo Granite along shear zones, where a episyenitization process took place under the influence of uranium and sodium-rich hydrothermal fluids.

Another important geological unit in the region is the Espinhaço Supergroup (not shown in Figure 1), comprising sandstones, conglomerates, siltstones, shales, quartzites and schists overlaying a sequence of 1.7 Ga rhyolites and rhyodacites. This supergroup is related to a basin developed during Upper Palaeoproterozoic rifting event. Tertiary and Quaternary alluvial sediments complete the geological setting of this region. According to [19] and [20] the geological and tectonic context of the Lagoa Real region is part of the evolution of the São Francisco Craton and of successive geological cycles: Jequié (Archean - with orogenic event around 2.7 Ga), Transamazonian (Palaeoproterozoic – with Orosirian orogenic event between 2.05 and 1.8 Ga), and Brasiliano (transition Neoproterozoic/Phanerozoic - with orogenic event around 0.54 +/- 0.1 Ga). During the latter cycle, Archean gneissic basement overthrusted metasediments of the Espinhaço Supergroup and therefore N-S regional thrust faults are found in Paramirim Block [21].

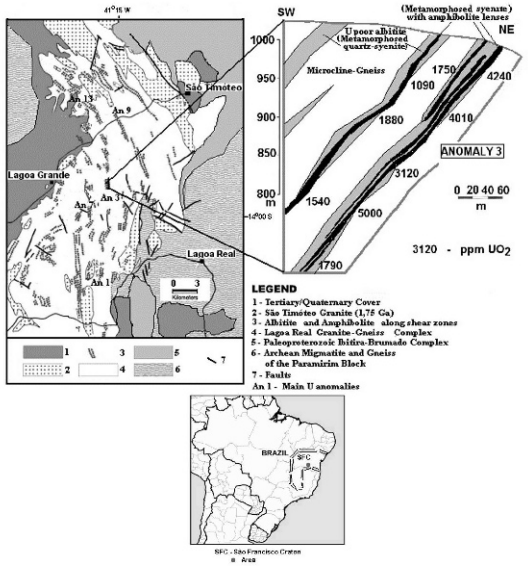

Figure 1. Geological map of the Lagoa Real uraniferous albitites, Bahia (BA-Brazil). Modified from [11] and [1]. Cross-section presents UO_2 contents in ppm for some mineralized levels of the anomaly 3, which represents one of 34 mineralized albitite with high uranium content of the Lagoa Real Uraniferous Province. In addition to surrounding microcline-gneisses, samples of amphibolites and mineralized albitites from anomalies 1, 3, 7, 9, and 13 (An1, An3, An7, An9, and An13) have been investigated in this work.

Uranium mineralization at Lagoa Real is found as finely disseminated (micro- to milimeter size) uraninite associated with discontinuous tabular bodies of albitites located along shear zones [1, 4, 7, 9, 13, 22]. Most bodies trend N40E to N30W and dip 30° to 90° to the southwest or northwest, with the exception of the northernmost

deposits, which dip to the east, and those situated in the central part of the region, which are almost vertical. Each body has maximum length of 3 km and average width of 10 m (max. 30 m). Mineralization extends up to 850 m below the surface as shown by drill cores. Bodies contain one or more mineralized levels, which may be interrupted in places. The contacts between mineralized levels with host gneissic rocks are abrupt (Figure 2). According to [1], amphibolites often occur along tabular bodies of albitites with the same structural trends and are also attained by shear zones.

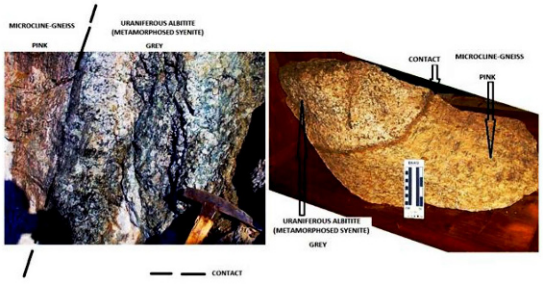

Figure 2. Sharp contacts between uraniferous albitite bodies and microcline-gneiss from Cachoeira Mine (anomaly 13).

Ore reserves at the Lagoa Real Uraniferous Province are presently reasonably well estimated at 94,000 tons of UO_2 and 6,700 tons of UO_2 of inferred reserves (CPRM/CBPM, 2003). Figure 1 inset shows a representative albitite vertical section, which presents UO_2 contents in ppm to some mineralized levels of the anomaly 3. These contents are similar to the main uranium anomalies of the province (between 1000 and 5000 ppm).

3. Methodology

In order to understand the genesis of the Lagoa Real uraniferous albitites, the following steps were undertaken:

1. a geological survey and sample collecting from Cachoeira Mine pit (anomaly 13) and drill-core rocks from anomalies 1, 3, 7, and 9 of the Lagoa Real Uraniferous Province (Fig. 1);

2. preparation of polished thin sections in the Sample Laboratory of the Development Center of Nuclear Technology (CDTN) for petrographic, microanalytical, and geochronologic studies;

3. interpretation of the physical and chemical properties of the fluid and melt inclusions.

The petrography of several rock types from the Lagoa Real region was carried out at the Fluid Inclusions and Metallogenesis Laboratory (LIF) of CDTN. A Leica DMR-XP microscope was used. Microanalyses of the mineral phases were carried out at the Physics Department of Minas Gerais Federal University (UFMG-Brazil) on a Jeol-JXA-8900 RL WD/ED Electron Microprobe. Quantitative WDS measurements have been done at analytical conditions of 15 Kv and 20 nA, with a 5 μm electron beam diameter, by using Smithsonian microbeam standards and x-ray lines described in [48]. Mössbauer spectroscopy of ^{57}Fe installed at CDTN provided support measures to the qualitative study of the Iron oxidation state in isolated mineral phases. These measurements were conducted at room temperature, atmospheric pressure and without external magnetic field in transmission geometry using a conventional Wissel spectrometer and a ^{57}Co/Rh source. Spectra were fitted by the least square method. Abbreviations used for names of rock-forming minerals are from [38].

For geochronological purposes, Pb/U isotope ratios in uraninite and zircon crystals of Lagoa Real albitites were determined by LA-ICP-MS technique (Laser Ablation Inductively Coupled Plasma Mass Spectrometry, reported by [23]) using zircon 91500 and uraninite TSA standards. The coupled Laser Ablation (Cetac/Geolas-Pro - operating wavelength 193 nm, energy density 40 J/cm^2 with spot size of 20 micrometers) and ICP-MS (Thermo/Element2 - sensitivity 1x10^9 cps/ppm In, mass resolution 600, 8,000, 20,000 FWHM, magnetic scan speed m/z 7 ->240 to 7 <150 ms, signal stability better than 2% over 1 hour) instruments used in this study are installed at the Memorial University of Newfoundland, St. John's - Canada. LA-ICP-MS analyses were performed with the same aforementioned polished thin sections. Common Pb has been corrected after [24] method and U-Pb diagrams have been made with the Isoplot software [25].

In order to understand the physical and chemical properties of the fluid and melt inclusions associated with the Lagoa Real albitite minerals, the following initial steps were undertaken: (1) mapping of fluid and melt inclusions in some mineral phases in Fluid Inclusions and Metallogenesis Laboratory (LIF) of CDTN. A Leica DMR-XP microscope was used. (2) microthermometric studies were carried out in LIF by using Chaixmeca heating/freezing system stage adapted to Leica DMR-XP microscope. The equipment was previously calibrated with conventional standards and natural fluid inclusions. The data are reproducible to ±0.2°C for the freezing runs and ±3°C for the heating runs. Fluid inclusions were analyzed after freezing the samples down to -160°C and heating them up to room temperature. Homogenization temperatures of fluid and melt inclusions were not measured but the latter ones did not melt during heating up to 450°C?. (3) analyses of the chemical contents of fluid and melt inclusions in

some minerals of the paragenesis associated to the uraniferous mineralization of Lagoa Real were performed by using the LA-ICP-MS technique with standard NIST 610 Glass Reference Material.

To be aware of petrological evolution of the Lagoa Real Uraniferous Province, 23 representative samples (five amphibolites, nine uraniferous albitites, and nine microcline-gneisses) from Cachoeira Mine pit (anomaly 13) and drill-core rocks from anomalies 1, 3, 7, and 9 were comminuted to lithogeochemistry studies by using a ring mill. ?Total abundances of the major oxides and some trace elements of 2 g of representative sample powder were fused in a metaborate/tetraborate mixture, dissolved in dilute nitric acid and analyzed at SGS Laboratories by Inductively Coupled Plasma Optical Emission Spectroscopy (major oxides) and Inductively Couple Plasma Mass Spectrometry (trace elements Zr and Th; U was not analyzed because it is assumed to have been mobile during the metamorphic events). The detection limits are generally around 0.01% for major oxides and 1ppm for trace elements. The precision of analysis is usually in the 1-2% RSD (relative standard deviation) range. Loss on ignition (LOI) was determined from the weight difference before and after tempering the powders at 1000°C for 60 minutes.

4. Petrography and mineral chemistry

Thirty representative polished thin sections of the amphibolites, albitites and microcline-gneisses of Lagoa Real Granitic-Gneissic Complex were investigated. This investigation led to a better understanding of the textures and mineral paragenesis related to each type as well as of the metamorphic reactions in the albitites. A plate of representative photomicrographs is given in the discussions and conclusions section. Electron microprobe analyses were carried out to determine the composition of the mineral phases. The fact that some of the analyses yielded totals below 100% indicates contents of OH, water and Fe^{3+} not detectable by the microprobe.

Amphibolites – Exhibit a predominantly nematoblastic texture, marked by preferred orientation of metamorphic pargasite crystals, associated with polygonalized oligoclase. These two minerals are responsible for 75% of the rock volume. Taramite was also found substituting pargasite and corresponds to 3% of the rock volume. The content of ilmenite and titanite is noticeable in this rock. Together, they represent almost 15% of the total volume. Allanite-(Ce), zircon, calcite and fluor-apatite complete the mineralogy. Table 1 shows the microanalyses of mineral phases of the amphibolites.

Albitites – The term albitite represents two distinct petrographic types in this work. Both are rich in albite, as the name indicates, and are closely related to ductile shear zones. The first one is a metamorphosed syenite without quartz but with associated uraniferous mineralization. The second one is a U-free metamorphosed quartz-syenite. The mineralogy is nearly the same for both petrographic types.

Micropetrographic studies indicated anisotropy in the metamorphic foliation. There are portions of the rock that keep the texture and mineralogy of the magmatic stage, including antiperthites. Other ones mix magmatic and metamorphic textures and many others have exclusively granoblastic texture (Figure 3).

Accessory minerals from magmatic portions are dark brown U-rich titanite [formula between $(Ca_{0.82}Fe^{+2}_{0.10}Pb_{0.08})(Ti_{0.57}U_{0.40}Al_{0.01}V_{0.01}Th_{0.01})(Si_{0.94}Al_{0.06})O_{4.40}(OH,F)_{0.60}$ and $(Ca_{0.93}Fe^{+2}_{0.05}Pb_{0.02})(Ti_{0.82}U_{0.07}Al_{0.05}V_{0.05}Th_{0.01})SiO_{4.65}(OH,F)_{0.35}$ – titanite crystals with high uranium concentrations have been reported by [26] and [10] and can be understood by the replacement between Ti^{4+} and U^{4+}, which have similar ionic radius], allanite-(Ce) with U and Th, magnetite, fluor-apatite, zircon, fluorite, and apophyllite. Magmatic calcite is sometimes present, which can be found between undeformed augite crystals. Table 2 shows the mineral microanalyses of the magmatic stage. Table 3 shows the chemical analyses of the recrystallized mineral phases and of the newly formed phases: oligoclase, aegirine-augite, microcline, calcite, titanite, allanite-(Ce), fluor-apatite, zircon, fluorite, andradite, hastingsite, epidote, biotite, hematite, and uraninite. Additionally, uraninite was found not only scattered through albitite but also inside recrystallized augite, hastingsite, andradite, calcite, biotite and epidote.

Microcline-gneisses – They vary from "augen" gneisses to less coarse types and represent the host rocks of the mineralized albitites. Microcline predominates (35 to 50% of the rock volume), followed by oligoclase and quartz (20 to 30% each). Hastingsite and biotite also appear. Together, they form 20% of the rock volume, both along with aegirine-augite. The opaque mineral is magnetite. Titanite, fluor-apatite, zircon, and allanite-(Ce) appear as accessory minerals. The microanalyses of these minerals are presented in Table 4.

5. U-Pb geochronology by LA-ICP-MS

Pb/U isotopic ratios obtained by LA-ICP-MS, which have shown to be reliable? in geochronological studies [31],

Table 1. Representative chemical analyses of amphibolite minerals obtained by electron microprobe. Fe^{2+} and Fe^{3+} proportions defined by Mössbauer Spectroscopy. Ion calculation according to [45]. Amphibole names according to [46].

Mineral Name	Pargasite	Oligoclase	Titanite	Ilmenite	Taramite	Allanite-(Ce)	Zircon	Fluor-Apatite	Calcite
SiO_2	43.58	60.17	29.20	1.44	43.12	35.57	31.88	0.00	0.00
TiO_2	0.74	0.00	38.56	51.42	0.00	0.00	0.00	0.00	0.00
Al_2O_3	11.91	24.32	0.00	0.00	20.85	21.43	0.19	0.00	0.00
FeO	16.75	0.00	0.00	44.35	10.41	11.93	0.00	0.00	0.00
Fe_2O_3	0.79	0.00	0.00	0.00	5.81	0.00	0.00	0.00	0.00
V_2O_3	0.00	0.00	0.00	0.00	0.89	0.00	0.00	0.00	0.00
MnO	0.33	0.00	0.00	0.00	0.19	0.41	0.00	0.00	0.00
MgO	9.27	0.00	0.00	0.00	6.36	0.00	0.00	0.00	0.00
CaO	11.98	6.25	27.74	1.73	2.48	20.01	0.37	54.51	58.25
Na_2O	1.59	8.88	0.00	0.00	6.10	0.00	0.00	0.00	0.00
K_2O	0.97	0.00	0.00	0.00	0.00	0.00	0.00	0.00	0.00
P_2O_5	0.00	0.00	0.00	0.00	0.00	0.00	0.00	41.55	0.00
F	0.00	0.00	0.00	0.00	0.00	0.00	0.00	2.25	0.00
ZrO_2	0.00	0.00	0.00	0.00	0.00	0.00	67.09	0.00	0.00
UO_2	0.00	0.00	0.00	0.00	0.00	0.00	0.32	0.00	0.00
PbO	0.00	0.00	0.55	0.00	0.00	0.48	0.00	0.00	0.00
ThO_2	0.00	0.00	0.00	0.00	0.00	0.31	0.00	0.00	0.00
Ce_2O_3	0.00	0.00	0.00	0.00	0.00	4.89	0.00	0.00	0.00
La_2O_3	0.00	0.00	0.00	0.00	0.00	3.39	0.00	0.00	0.00
Nd_2O_3	0.00	0.00	0.00	0.00	0.00	0.60	0.00	0.00	0.00
CO_2	0.00	0.00	0.00	0.00	0.00	0.00	0.00	0.00	41.75
Total	97.91	99.62	96.05	98.94	96.21	99.02	99.85	98.31	100.00
Oxygens	23	32	20	6	23	12	16	13	6
	Si 6.53	Si 10.78	Si 3.99	Si 0.07	Si 6.49	Si 2.93	Si 3.92	Ca 5.07	Ca 2.12
	Al 1.47	Al 5.13	Ti 3.97	Ti 1.95	Al 1.51	Al 2.08	Al 0.03	P 3.17	C 1.94
	Al 0.64	Ca 1.20	Ca 4.06	Fe2 1.87	Al 2.19	Fe2 0.82	Ca 0.05	F 1.28	-
	Fe3 0.11	Na 3.08	Pb 0.02	Ca 0.09	Fe3 0.87	Mn 0.03	Zr 4.02	-	-
	Ti 0.08	K 0.00	-	-	V 0.11	Ca 1.76	U 0.01	-	-
I	Mg 2.07	-	-	-	Mg 1.43	Pb 0.01	-	-	-
O	Fe2 2.08	-	-	-	Fe2 0.40	Th 0.01	-	-	-
N	Mn 0.02	-	-	-	Mn 0.01	Ce 0.15	-	-	-
S	Fe2 0.01	Ab 75	-	-	Fe2 0.78	La 0.10	-	-	-
	Mn 0.02	An 25	-	-	Mn 0.01	Nd 0.02	-	-	-
	Ca 1.93	Or 0	-	-	Ca 0.40	-	-	-	-
	Na 0.04	-	-	-	Na 0.81	-	-	-	-
	Na 0.42	-	-	-	Na 0.97	-	-	-	-
	K 0.19	-	-	-	-	-	-	-	-

allowed the age determination of magmatic and metamorphic events that resulted in the formation of the uraninite of the Lagoa Real Granitic-Gneissic Complex.

Rim and core areas of two zircon crystals from microcline-gneisses, host rocks of uraniferous metamorphosed syenites from radioactive anomaly 13 (Cachoeira Mine), produced the U-Pb discordia of Figure 4, anchored to 0 Ma (probable recent Pb loss). In this figure, one finds the values of Pb/U ratios of each zircon. The age of 2,009 +/- 78 Ma corresponding to the upper intercept is interpreted as being the magmatic crystallization of granitoids, which represent the parent rocks of the microcline-gneisses. Palaeoproterozoic ages around 2.0 Ga have been found for the magmatism associated with the Orosirian Orogen-

Table 2. Representative chemical analyses of former magmatic minerals in the metamorphosed syenites, obtained by electron microprobe. Fe^{2+} and Fe^{3+} proportions were measured by Mössbauer Spectroscopy. Ion calculation according to [45]. Two uraniferous titanite represent the observed range of UO_2 content.

Mineral Name	Albite	Iron-rich augite	Microcline	Calcite	Magnetite	U-rich Titanite	U-rich Titanite	Allanite-(Ce)	Fluor-Apatite	Zircon	Fluorite	Apophyllite
SiO_2	69.19	52.78	64.01	0.00	0.00	19.34	27.67	34.53	0.00	33.88	0.00	51.45
TiO_2	0.00	0.10	0.00	0.00	0.00	16.04	29.46	0.00	0.00	0.00	0.00	0.00
Al_2O_3	19.30	0.89	18.41	0.00	0.00	2.02	1.26	13.40	0.00	0.00	0.00	0.00
FeO	0.00	10.02	0.00	0.00	30.11	1.84	1.76	12.09	0.00	0.00	0.00	0.00
Fe_2O_3	0.00	3.10	0.00	0.00	66.70	0.00	0.00	3.40	0.00	0.00	0.00	0.00
V_2O_3	0.00	0.65	0.00	0.00	2.23	0.05	1.53	0.00	0.00	0.00	0.00	0.00
MnO	0.00	0.35	0.00	0.00	0.00	0.00	0.00	0.00	0.00	0.00	0.00	0.00
MgO	0.00	9.29	0.00	0.00	0.00	0.00	0.00	0.00	0.00	0.00	0.00	0.00
CaO	0.26	20.83	0.06	56.34	0.00	15.79	23.80	13.23	52.49	0.00	52.39	24.78
Na_2O	11.29	2.07	0.77	0.00	0.00	0.00	0.00	0.00	0.00	0.00	0.00	0.00
K_2O	0.00	0.00	15.85	0.00	0.00	0.00	0.00	0.00	0.00	0.00	0.00	5.09
P_2O_5	0.00	0.00	0.00	0.00	0.00	0.00	0.00	0.00	40.97	0.00	0.00	0.00
F	0.00	0.00	0.00	0.00	0.00	0.20	0.59	0.25	2.22	0.00	46.94	1.13
ZrO_2	0.00	Q 1,68	0.00	0.00	0.00	0.00	0.00	0.00	0.00	65.98	0.00	0.00
UO_2	0.00	J 0,30	0.00	0.00	0.00	38,14 (UO_2 Max)	8,71 (UO_2 Min)	1.30	0.00	0.12	0.00	0.00
PbO	0.00	Wo 45	0.00	0.00	0.00	3.51	2.63	0.51	0.00	0.08	0.00	0.00
ThO2	0.00	En 30	0.00	0.00	0.00	0.69	0.07	0.68	0.00	0.00	0.00	0.00
Ce_2O_3	0.00	Fs 25	0.00	0.00	0.00	0.00	0.00	10.39	2.26	0.00	0.00	0.00
La_2O_3	0.00	WEF 85	0.00	0.00	0.00	0.00	0.00	3.71	0.91	0.00	0.00	0.00
Nd_2O_3	0.00	Jd 4	0.00	0.00	0.00	0.00	0.00	2.64	0.63	0.00	0.00	0.00
CO_2	0.00	Ae 11	0.00	43.66	0.00	0.00	0.00	0.00	0.00	0.00	0.00	0.00
Total	100.04	100.08	99.10	100.00	99.04	97.62	97.48	96.13	99.48	100.06	99.33	82,45(+H_2O)
Oxygens	32	6	32	6	4	20	20	12	13	16	-	20
	Si 12,05	Si 1,99	Si 11,94	Ca 2,01	Fe_2 0,98	Si 3,75	Si 4,09	Si 3,05	Ca 5,04	Si 4,10	Ca 0,95	Si 7,76
	Al 3,96	Al 0,01	Al 4,05	C 1,99	Fe_3 1,95	Al 0,46	Al 0,22	Al 1,40	Ce 0,07	Zr 3,90	F 2,05	Ca 4,00
	Ca 0,05	Al 0,04	Ca 0,01	-	V 0,07	V 0,01	V 0,18	Fe_3 0,25	La 0,03	U 0,00	-	K 0,98
I	Na 3,81	Ti 0,01	Na 0,28	-	-	Ti 2,34	Ti 3,28	Fe_2 0,90	Nd 0,02	Pb 0,00	-	F 1,08
O	K 0,00	V 0,02	K 3,77	-	-	U 1,65	U 0,29	U 0,03	P 3,11	-	-	-
N	-	Fe_3 0,10	-	-	-	Ca 3,28	Ca 3,77	Ca 1,25	F 1,26	-	-	-
S	-	Fe_2 0,31	-	-	-	Fe_2 0,30	Fe_2 0,22	Pb 0.01	-	-	-	-
	Ab 99	Mg 0,52	Ab 07	-	-	Pb 0,18	Pb 0,10	Th 0.01	-	-	-	-
	An 01	Mn 0,01	An 00	-	-	Th 0,03	Th 0,00	Ce 0,34	-	-	-	-
	Or 00	Ca 0,84	Or 93	-	-	-	-	La 0,12	-	-	-	-
	-	Na 0,15	-	-	-	-	-	Nd 0,08	-	-	-	-

Table 3. Representative chemical analyses of metamorphic minerals from metamorphosed syenites obtained by electron microprobe. Fe^{2+} and Fe^{3+} proportions defined by Mössbauer Spectroscopy. Ion calculation according to [45]. Amphibole naming according to [46].

Mineral Name	Oligoclase	Aegirine- Augite	Microcline	Calcite	Titanite	Allanite-(Ce)	Fluor-Apatite	Zircon	Fluorite	Andradite	Hastingsite	Epidote	Biotite	Uraninite	Hematite
SiO_2	65.21	52.04	65.24	0.00	30.51	38.35	1.09	34.47	0.00	37.12	41.11	37.91	38.89	1.75	0.00
TiO_2	0.00	0.00	0.00	0.00	34.28	0.00	0.00	0.00	0.00	0.40	0.45	0.00	0.68	0.00	0.00
Al_2O_3	20.49	2.55	18.83	0.00	1.05	16.22	0.00	0.00	0.00	3.39	11.38	20.78	12.95	0.00	0.00
FeO	0.00	6.02	0.00	0.00	1.82	12.66	0.00	0.00	0.00	0.00	9.51	0.00	13.32	0.00	0.00
Fe_2O_3	0.00	9.04	0.00	0.00	0.00	2.78	0.00	0.00	0.00	23.04	10.10	16.30	3.33	0.00	98.32
V_2O_3	0.00	0.00	0.00	0.00	1.73	0.00	0.00	0.00	0.00	1.88	0.00	0.00	0.22	0.00	0.00
MnO	0.00	0.13	0.00	0.00	0.00	0.00	0.00	0.00	0.00	1.01	0.48	0.00	0.19	0.00	0.00
MgO	0.00	7.75	0.00	0.00	0.00	0.00	0.00	0.00	0.00	0.00	9.12	0.00	14.86	0.00	0.00
CaO	2.63	18.10	0.35	56.53	28.42	16.75	55.28	0.00	51.27	32.78	10.41	23.35	0.00	3.98	0.00
Na_2O	10.59	4.12	1.12	0.00	0.00	0.00	0.00	0.00	0.00	0.00	3.15	0.00	0.00	0.00	0.00
K_2O	0.00	0.00	14.93	0.00	0.00	0.00	0.00	0.00	0.00	0.00	2.35	0.00	11.04	0.00	0.00
P_2O_5	0.00	0.00	0.00	0.00	0.00	0.00	39.93	0.00	0.00	0.00	0.00	0.00	0.00	0.00	0.00
F	0.00	0.00	0.00	0.00	0.47	0.16	2.24	0.00	48.68	0.00	0.00	0.00	1.54	0.00	0.00
ZrO_2	0.00	Q 1,35	0.00	0.00	0.00	0.00	0.00	63.24	0.00	0.00	0.00	0.00	0.00	0.00	0.00
UO_2	0.00	J 0,60	0.00	0.00	0.00	0.00	0.00	0.00	0.00	0.00	0.00	0.00	0.00	85.60	0.00
PbO	0.00	Wo 42	0.00	0.00	0.00	0.43	0.00	0.00	0.00	Alm 0	0.00	0.40	0.00	6.40	0.00
ThO_2	0.00	En 28	0.00	0.00	0.00	0.50	0.00	0.00	0.00	And 76	0.00	0.00	0.00	0.00	0.00
Ce_2O_3	0.00	Fs 30	0.00	0.00	0.00	4.56	0.72	0.00	0.00	Gros 15	0.00	0.00	0.00	0.00	0.00
La_2O_3	0.00	WEF 69	0.00	0.00	0.00	1.61	0.21	0.00	0.00	Pyr 0	0.00	0.00	0.00	0.00	0.00
Nd_2O_3	0.00	Jd 6	0.00	0.00	0.00	1.42	0.09	0.00	0.00	Spes 2	0.00	0.00	0.00	0.00	0.00
CO_2	0.00	Ae 25	0.00	43.47	0.00	0.00	0.00	0.00	0.00	Gold 7	0.00	0.00	0.00	0.00	0.00
Total	98.92	99.75	100.47	100.00	98.28	95.44	99.56	97.71	99.95	99.62	98.06	98.74	97.02	97.73	98.32
Oxygens	32	6	32	6	20	12	13	16	-	12	23	12	24	2	3
	Si 11,61	Si 1,95	Si 11,95	Ca 2,03	Si 4,11	Si 3,07	Ca 4,85	Si 4,22	Ca 0,98	Si 3,09	Si 6,37	Si 2,91	Si 6,16	Si 0,07	Fe_3 2,00
	Al 4,30	Al 0,05	Al 4,05	C 1,99	Al 0,17	Al 1,73	Ce 0,02	Zr 3,78	F 2,01	Al 0,00	Al 1,63	Al 1,88	Ti 0,08	U 0,80	-
	Ca 0,50	Al 0,06	Ca 0,07	-	V 0,18	Fe_3 0,20	La 0,01	-	-	AlIV 0,33	Al 0,45	Fe_3 0,94	Al 2,42	Ca 0,18	-
	Na 3,66	Ti 0,00	Na 0,40	-	Ti 3,47	Fe_2 0,90	Nd 0,00	-	-	Fe_3 1,44	Fe_3 1,22	Ca 1,92	V 0,03	Pb 0,07	-
I	K 0,00	V 0,00	K 3,49	-	U 1,65	U 0,00	P 2,77	-	-	Ti 0,03	Ti 0,05	Pb 0,01	Fe_3 0,41	-	-
O	-	Fe_3 0,28	-	-	Ca 4,10	Ca 1,63	F 1,16	-	-	V 0,12	Mg 2,11	-	Fe_2 1,80	-	-
N	-	Fe_2 0,19	-	-	Fe_2 0,20	Pb 0.01	-	-	-	Mn 0,07	Fe_2 1,14	-	Mn 0,03	-	-
S	Ab 90	Mg 0,43	Ab 10	-	-	Th 0.01	-	-	-	Ca 2,92	Mn 0,03	-	Mg 3,51	-	-
	An 10	Mn 0,01	An 02	-	-	Ce 0,14	-	-	-	-	Fe_2 0,10	-	K 2,23	-	-
	Or 00	Ca 0,73	Or 88	-	-	La 0,05	-	-	-	-	Mn 0,03	-	F 1,54	-	-
	-	Na 0,30	-	-	-	Nd 0,04	-	-	-	-	Ca 1,73	-	-	-	-
	-	-	-	-	-	-	-	-	-	-	Na 0,14	-	-	-	-
	-	-	-	-	-	-	-	-	-	-	Na 0,80	-	-	-	-
	-	-	-	-	-	-	-	-	-	-	K 0,47	-	-	-	-

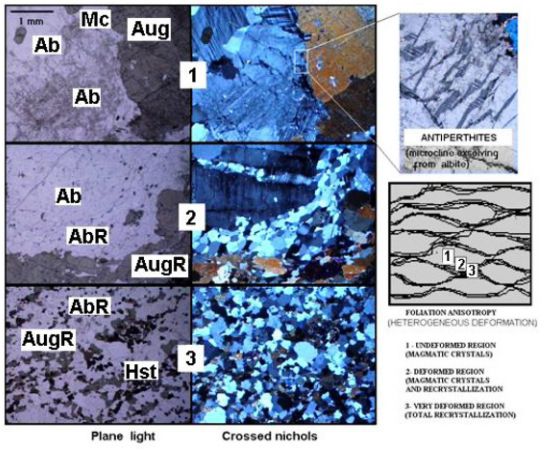

Figure 3. Photomicrographs of the metamorphosed syenites (plane-polarized light and crossed nicols). 1 - Igneous texture and antiperthites show the magmatic stage, corresponding to region 1 of the schematically displayed foliation anisotropy in the right side of the figure. 2 - Recrystallization of a large albite crystal, associated with recrystallized iron-rich augite suggests the initial stages of the metamorphic recrystallization (region 2 in the scheme). 3 - Well developed granoblastic textures indicate the final stages of the metamorphic recrystallization (region 3 with strongest deformation in the scheme). Metamorphic hastingsite appears in region 3 (Ab – Magmatic albite, Aug – Magmatic augite, Mc – Magmatic microcline, AbR – Albite recrystallized during metamorphism, AugR – Augite recrystallized during metamorphism, Hst – hastingsite).

esis in several regions of the São Francisco Craton [32, 33].

The Pb/U ratios of rim and core zones of three zircon crystals from metamorphosed syenites of three different radioactive anomalies (3, 7, and 13) produced the U-Pb discordia of Figure 5, which also shows the values of the Pb/U ratios of each zircon and its crystal zone. Zircon data show how the grains have lost varied amounts of lead with time, i.e., the classic discordia from original age to closure. The age of 1,904 +/- 44 Ma, corresponding to the upper intercept, can be interpreted either as magmatic crystallization and/or as influence of Orosirian metamorphism. The age of 483 +/- 100 Ma, corresponding to the lower intercept, is interpreted as imprint of the Brasiliano metamorphism on the zircon U-Pb system during the reactivation of the shear zones where the metamorphosed syenites are found. [21] and [12] showed the result of the Brasiliano event on the Lagoa Real Granitic-Gneissic Complex.

Assuming? that the uraninite grains were formed during metamorphic events, the Pb/U isotopic ratios to these minerals were also determined. Andradite-related uraninite and epidote-related uraninite were analysed. $^{207}Pb/^{235}U$ is around 0.7 for the andradite-related uraninite and around 0.3 for the epidote-related uraninite grains. The

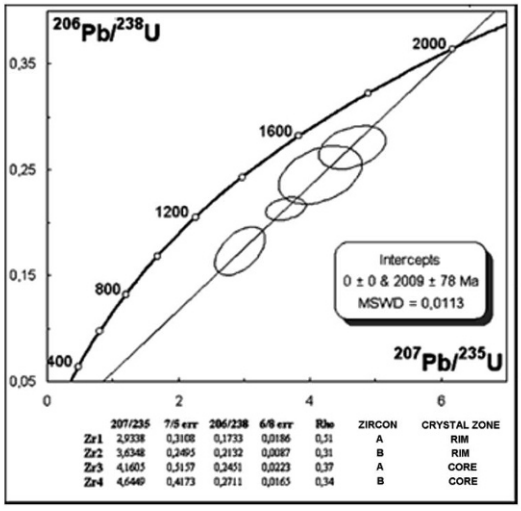

Figure 4. U-Pb discordia anchored to 0 Ma to zircons of microcline-gneisses. Analysed crystal zones are shown. Error ellipses are 2σ.

U-Pb discordia of these two populations of uraninite anchored to 0 Ma are given in Figure 6 along with the values of Pb/U ratios of each grain analysed.

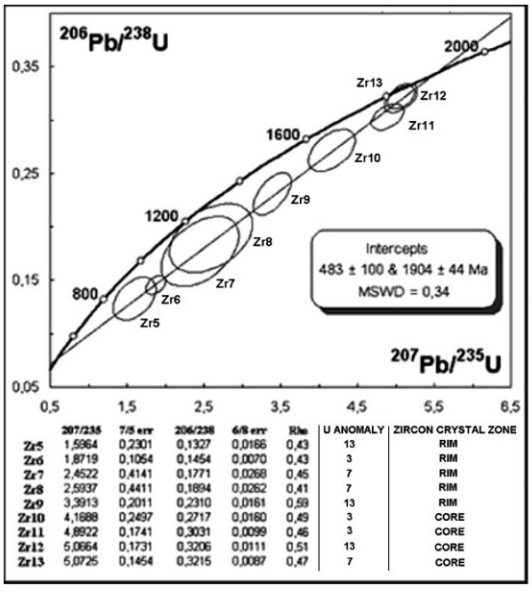

Figure 5. U-Pb discordia to zircons of metamorphosed syenites (uraniferous albitites) from anomalies 3, 7, and 13. Analysed crystal zones are shown. Error ellipses are 2σ.

The first uraninite population shows a U-Pb system starting during a 1,868 +/- 69 Ma metamorphic episode. This Palaeoproterozoic age could be attributed to the peak of the metamorphism that accompanied the development of the shear zones created during the final stages of the

Table 4. Representative chemical analyses of minerals found in the microcline-gneisses, obtained by electron microprobe. Fe^{2+} and Fe^{3+} proportions defined by Mössbauer Spectroscopy. Ion calculation according to [45]. Amphibole name according to [46].

Mineral Name	Microcline	Oligoclase	Quartz	Hastingsite	Biotite	Aegirine-Augite	Magnetite	Titanite	Allanite-(Ce)	Fluor-Apatite	Zircon
SiO_2	63.92	65.62	99.03	38.34	34.13	50.87	0.00	30.87	38.15	0.00	32.04
TiO_2	0.00	0.00	0.00	0.00	2.03	0.00	0.00	30.04	0.00	0.00	0.00
Al_2O_3	18.75	21.31	0.00	13.13	15.55	1.45	0.00	6.17	15.44	0.00	0.00
FeO	0.00	0.00	0.00	25.11	28.04	13.30	29.82	0.00	17.41	0.00	0.00
Fe_2O_3	0.00	0.00	0.00	5.51	4.56	10.04	69.50	1.66	0.00	0.00	0.00
V_2O_3	0.00	0.00	0.00	0.00	0.00	0.00	0.00	0.00	0.00	0.00	0.00
MnO	0.00	0.00	0.00	0.86	0.79	0.32	0.00	0.00	0.00	0.00	0.00
MgO	0.00	0.00	0.00	1.77	4.23	3.65	0.00	0.00	0.00	0.00	0.00
CaO	0.00	2.16	0.00	10.79	0.00	15.77	0.00	29.01	14.80	55.01	0.00
Na_2O	0.26	10.69	0.00	1.36	0.00	4.38	0.00	0.00	0.00	0.00	0.00
K_2O	16.04	0.20	0.00	2.20	8.81	0.00	0.00	0.00	0.00	0.00	0.00
P_2O_5	0.00	0.00	0.00	0.00	0.00	0.00	0.00	0.00	0.00	42.06	0.00
F	0.00	0.00	0.00	0.00	0.00	0.00	0.00	0.00	0.00	2.04	0.00
ZrO_2	0.00	0.00	0.00	0.00	0.00	Q 1,30	0.00	0.00	0.00	0.00	66.57
UO_2	0.00	0.00	0.00	0.00	0.00	J 0,66	0.00	0.00	0.00	0.00	0.00
PbO	0.00	0.00	0.00	0.00	0.00	Wo 40	0.00	0.00	0.00	0.00	0.00
ThO_2	0.00	0.00	0.00	0.00	0.00	En 13	0.00	0.00	0.24	0.00	0.00
Ce_2O_3	0.00	0.00	0.00	0.00	0.00	Fs 47	0.00	0.00	6.87	0.36	0.00
La_2O_3	0.00	0.00	0.00	0.00	0.00	WEF 67	0.00	0.00	3.86	0.21	0.00
Nd_2O_3	0.00	0.00	0.00	0.00	0.00	Jd 4	0.00	0.00	0.00	0.00	0.00
CO_2	0.00	0.00	0.00	0.00	0.00	Ae 30	0.00	0.00	0.00	0.00	0.00
Total	98.97	99.98	99.03	99.07	98.14	99.78	99.32	97.75	96.77	99.68	98.61
Oxygens	32	32	2	23	24	6	4	20	12	13	16
	Si 11,93	Si 11,55	Si 1,00	Si 6,06	Si 5,66	Si 1,97	Fe_2 0,97	Si 4,09	Si 3,27	Ca 4,77	Si 3,97
	Al 4,12	Al 4,42	-	Al 1,94	Ti 0,25	Al 0,03	Fe_3 2,02	Al 0,97	Al 1,56	Ce 0,01	Zr 4,03
	Ca 0,00	Ca 0,41	-	Al 0,50	Al 3,04	Al 0,04	-	Fe_3 0,17	Fe_3 0,00	La 0,01	-
	Na 0,09	Na 3,65	-	Fe_3 0,76	V 0,0	Ti 0,00	-	Ti 3,00	Fe_2 1,25	Nd 0,00	-
	K 3,82	K 0,05	-	Ti 0,00	Fe_3 0,62	V 0,00	-	Ca 4,10	U 0,00	P 2,88	-
	-	-	-	Mg 0,42	Fe_2 3,90	Fe_3 0,32	-	-	Ca 1,36	F 1,04	-
I	-	-	-	Fe_2 3,26	Mn 0,11	Fe_2 0,43	-	-	Pb 0,00	-	-
O	Ab 02	Ab 89	-	Mn 0,06	Mg 1,05	Mg 0,21	-	-	Th 0,01	-	-
N	An 00	An 10	-	Fe_2 0,02	K 1,86	Mn 0,01	-	-	Ce 0,22	-	-
S	Or 98	Or 01	-	Mn 0,06	-	Ca 0,66	-	-	La 0,12	-	-
	-	-	-	Ca 1,83	-	Na 0,33	-	-	Nd 0,0	-	-
	-	-	-	Na 0,09	-	-	-	-	-	-	-
	-	-	-	Na 0,33	-	-	-	-	-	-	-
	-	-	-	K 0,44	-	-	-	-	-	-	-

Orosirian Orogenesis, either simultaneously or immediately after the crystallization of the uraniferous syenites (considering age errors). The absence of age data related to the Brasiliano event is probably caused by recent Pb loss.

Within the age errors (605 +/- 170 Ma), uraninite grains of the second population seem to have been crystallized during the Brasiliano metamorphic event, which is well recorded by the lower intercept of the zircon U-Pb discordia of uraniferous metasyenites at 483 +/- 100 Ma (Figure 5).

It is obvious to interpret the two metamorphic foliations with planar surfaces oblique to each other within the microcline-gneisses of the Lagoa Real Complex [1] as be-

ing of Orosirian and of Brasiliano origin.

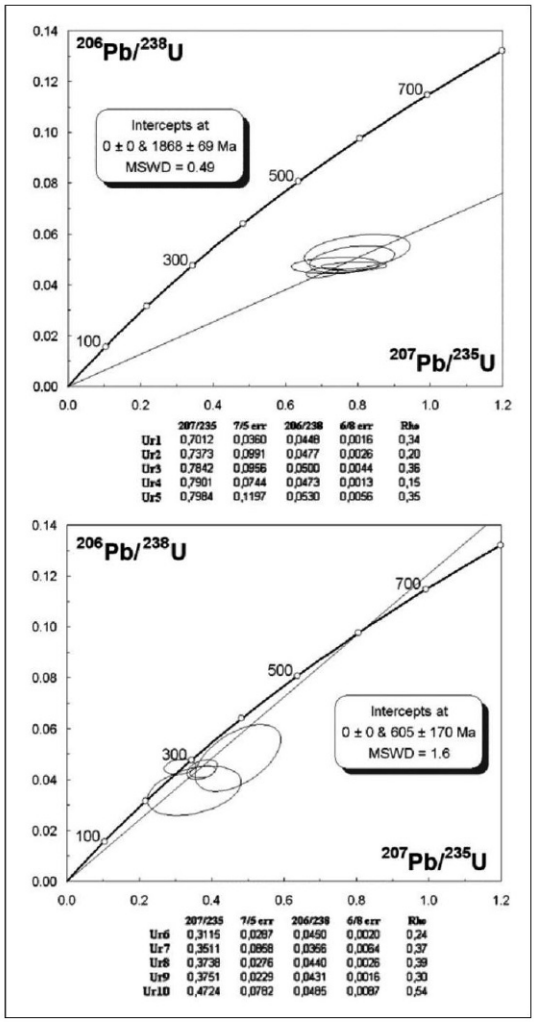

Figure 6. U-Pb discordias anchored to 0 Ma of two populations of uraninites of metamorphosed syenites (uraniferous albitites). Error ellipses are 2σ for the older ones and 1σ for the younger ones.

6. Fluid and melt inclusions by LA-ICP-MS and microthermometry

Chemical content of fluid and melt inclusions in some minerals of the paragenesis related to the uraniferous mineralization of Lagoa Real were qualitatively analysed by LA-ICP-MS (Laser Ablation Inductively Coupled Plasma Mass Spectrometry). This technique has proven to be extremely effective in chemical studies of fluid and melt inclusions in minerals [34]. The graphic interpretation of the ICP-MS signals was done as follows: background means standard signal intensity, which increases when the laser ablated the host mineral. The next change in signal intensity means that the laser ablated a melt or fluid inclusion.

The presence of iron-rich augite in the magmatic stage of metamorphosed syenites (uraniferous albitites) is confirmed by its melt inclusions as well as by zoned structures found in some augite crystals. Melt inclusions contain a pale brown monophase solid. The ICP-MS signals show that melt inclusions are richer in Na, Al and Ti than augite itself (Figure 7). The magma contained these elements when augite crystallized and they were consumed by albite (Na and Al) and uraniferous titanite (Ti) during syenite crystallization processes. The melt inclusions also contain Nb, Rb, and Ba, which are incompatible in the main silicate minerals of the rock. It is interesting to note that the content of Ca and Sr is smaller in melt inclusions than in augite itself because these elements are compatible with the augite structure. Some radiogenic lead in augite reveals the presence of U in the syenite magma.

In order to get some ideas about the magmatic fluids, the primary three-phase fluid inclusions in augite crystals of the magmatic stage of the metamorphosed uraniferous syenite (uraniferous albitite) were analysed (solid crystalline phase-S, vapour phase-V, and aqueous phase-L). The diagram in Figure 8 shows that the primary fluid inclusion in magmatic iron-rich augite of the albitite contains Na, Rb, and Ba (Rb and Ba are incompatible to the syenite minerals and remained in the fluid phase). Microthermometric studies point to a very low initial melting temperature, between -69.7°C and -62.6°C (Table 5), which is probably caused by the presence of Rb and Ba in this complex saline system, certainly of magmatic origin. Fluorine (inferred from the presence of fluorite in rock), rubidium and barium lower the stability of the fluid phase down to very low eutectic melting temperatures.

Fluid inclusions in garnet and recrystallized apatite were also analysed in order to determine the fluids within the metamorphosed syenites and andradite with uraninite inclusions. The fluid inclusions in garnet normally have either four phases (L, V, and two S – dark-orange and colorless) or three phases (L, V, and either colorless S or dark-orange S) and recrystallized apatite contains either two phases (V-L) or one phase (L) inclusions. It is worth pointing out that apparent solid (remnant melt?) inclusions were identified in recrystallized apatite.

The formation of andradite from iron-rich augite during shear events contemporary with the metamorphosed syenites is certified by the ICP-MS signals presented in Figure 9. The elements Si, Ca, Ti, V, Fe, Na, Mg, Al, and Sr that can enter the structure of the magmatic augite were found in garnet, with the exception of Mg and Na, which

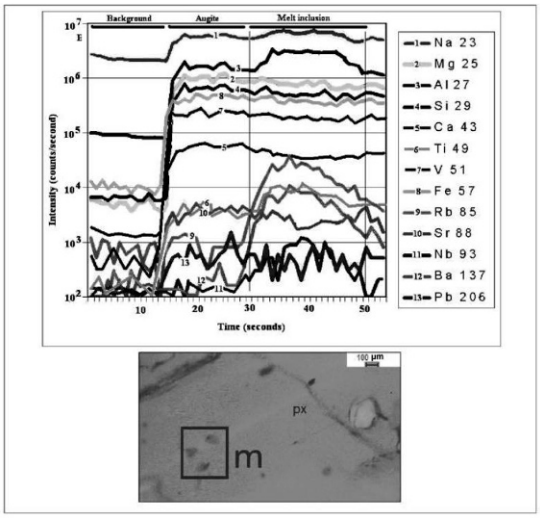

Figure 7. ICP-MS signals of magmatic iron-rich augite from syenite (uraniferous albitite) and of its pale brown solid monophasic melt (m) inclusions (photomicrograph inset; px = augite pyroxene). Logarithmic intensity scale.

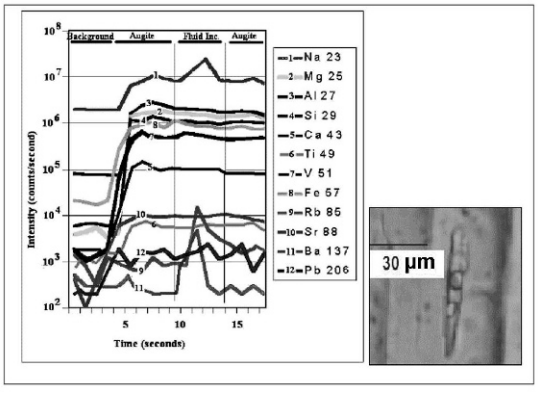

Figure 8. ICP-MS signals of magmatic iron-rich augite from syenite (uraniferous albitite) and of its primary three-phase fluid inclusion (photomicrograph inset). Logarithmic intensity scale.

preferentially went into the fluid phase. Besides Mg and Na, Rb, Ba, U (^{235}U and ^{238}U) and associated radiogenic Pb were also found.

Uranium released from magmatic titanite during the 1.9 Ga metamorphism was recorded in the fluid inclusions in andradite, which probably formed simultaneously with the recrystallized titanite. This also caused the disseminated uraninite inside andradite. Furthermore, the dark-orange crystal inside the fluid inclusions of andradite (Figure 9) probably contains radiogenic Pb.

The material released during one of the laser ablations of recrystallized apatite produced the ICP-MS signals presented in Figure 10. The laser ablated the apatite, two

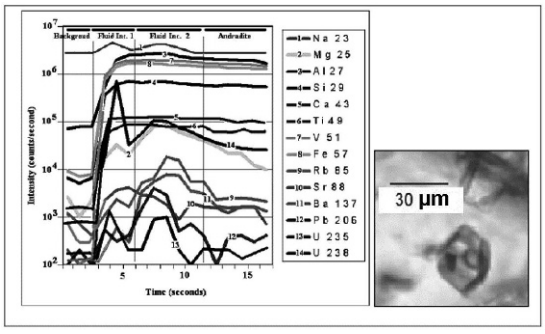

Figure 9. ICP-MS signals of andradite garnet of the metamorphic stage, which generated metamorphosed syenites (uraniferous albitites) and two of its fluid inclusions. One representative four-phase fluid inclusion (2 solid phases – one of them is dark-orange and the other one is colorless, 1 liquid phase, and 1 vapour phase, see photomicrograph inset) in andradite is shown in photo. Logarithmic intensity scale.

fluid inclusions, and a probable remnant solid inclusion. P, Ca, Sr, V, and the rare earth elements (La, Ce, Nd, Sm) result from apatite. The rare earth elements and thorium are the main constituents of the solid inclusion. The content of the fluid inclusions in recrystallized apatite is the same as those of the garnet fluid inclusions. Together with initial melting temperatures between -53.7°C and -49.5°C (Table 5) this suggests that andradite crystallized together with recrystallized apatite in the same metamorphic event.

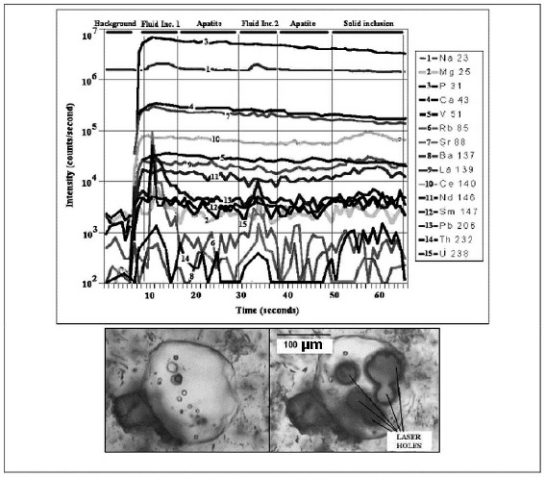

Figure 10. ICP-MS signals of recrystallized apatite of the metamorphic stage, which generated metamorphosed syenites (uraniferous albitites). The ICP-MS signals of two of its fluid inclusions and of a solid inclusion are also presented. Monophase and two-phase fluid inclusions in recrystallized apatite from a metamorphosed syenite before (left) and after (right) laser ablation are shown (photomicrograph inset). Logarithmic intensity scale.

Table 5. Microthermometric data of fluid inclusions (FI) in augite, andradite and apatite from Lagoa Real metamorphosed syenite (uraniferous albitite).

FI	AUGITE				ANDRADITE		APATITE	
	Primary fluid inclusions (yielded during magmatic stage)		Secondary fluid inclusions (yielded during metamorphic stage)		Fluid inclusions yielded during metamorphic stage		Fluid inclusions yielded during metamorphic stage	
	Initial ice-melting temperature (°C)	Final ice-melting temperature (°C)	Initial ice-melting temperature (°C)	Final ice-melting temperature (°C)	Initial ice-melting temperature (°C)	Final ice-melting temperature (°C)	Initial ice-melting temperature (°C)	Final ice-melting temperature (°C)
1	-64.0	-12.0	-52.5	-12.2	-53.0	-12.0	-49.5	-9.0
2	-65.4	-11.5	-52.3	-15.0	-52.1	-11.6	-51.4	-8.4
3	-63.8	-11.7	-52.7	-11.5	-52.0	-11.9	-51.7	-10.7
4	-62.6	-11.4	-55.0	-11.0	-52.1	-11.6	-50.0	-10.1
5	-64.4	-11.1	-50.9	-11.2	-53.5	-9.3	-49.9	-11.6
6	-65.5	-13.1	-52.2	-11.5	-53.1	-11.7	-52.4	-9.5
7	-64.2	-12.1	-52.0	-12.0	-51.7	-13.3	-51.0	-8.9
8	-66.2	-12.1	-55.0	-11.2	-52.5	-13.0	-53.7	-9.2
9	-69.7	-11.4	-54.9	-13.0	-51.6	-9.6	-50.2	-10.0

7. Lithogeochemistry

Contents of major (weight %) and trace elements (ppm) of the three different rock types are presented in Table 6. CIPW normative mineral content was calculated by the Minpet software [35]. Although the analysed rocks are metamorphic, CIPW data are presented in Table 6 in order to draw some conclusions about the igneous protoliths. Note that the higher LOI of samples Ab1, Ab2 and Ab18 is due to the presence of uranophane (hydrated mineral). A/X versus B/X Pearce diagrams [36] are useful tools to prove whether supposedly mobile elements such as Na and K from albitites and microcline-gneiss were immobile during metamorphism. In the diagrams X represents Zr (immobile normalizing element), B silica and A alkalis (Na_2O and K_2O). Irregular patterns and linear trends indicate element mobilization or immobility during metamorphism respectively. The linear trends in Figure 11 show that both Na and K were not mobilized during metamorphism of albitites and microcline-gneiss. Another way to test element mobilization is the chemical index of alteration (CIA [47]), which is calculated as CIA = $Al_2O_3/(Al_2O_3+CaO^*+Na_2O+K_2O)]^*100$; the elemental abundances are expressed as molar proportions, and CaO^* represents the CaO content of the silicate fraction. Only calcite-free, low CaO albitite samples Ab23, Ab30 and Ab31 have been used for CIA calculations, resulting in values around 47, which is in the range of igneous rocks (45-55). CIA values of all Mgn# samples in Table 6 range between 45 and 55.

We have shown that there is no important mobilization of alkalis. Therefore the metamorphic rocks can be treated as their igneous protoliths. In the total alkali versus silica diagram (TAS, Figure 12 [37]), amphibolite protolith is an alkali-diorite and albitite protolith is an alkaline rock ranging from syenodiorite to syenite. Furthermore, in S1, S2, S3, and T fields from Figure 12, rocks belonging to transalkali suite of [39] must be classified as "sodic" if $Na_2O - 2.0 > K_2O$ or "potassic" if $Na_2O - 2.0 < K_2O$ after [40]. Three of five alkali-diorite samples are sodic as well as all of the nine syenodiorite (albitite protolith) samples. The Microcline-gneiss protolith, however, is a potassic subalkaline syenogranite.

Harker diagrams with silica versus major oxides (Figure 13) and silica versus trace elements (Figure 14) show the petrogenetic relation between alkali-diorite and syenitic rocks. Increasing silica content is accompanied by decreasing amounts of Ti, Fe, Mg, Ca, P, and increasing of Al, Na (hence albite, not K-feldspar, is

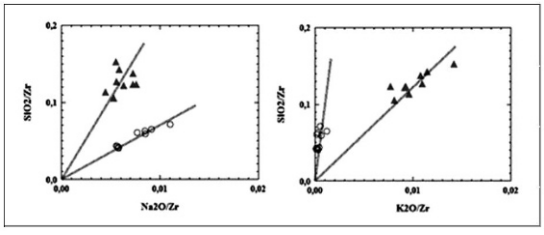

Figure 11. Linear trends for Na and K in the Pearce diagrams [36] suggest no representative alkalis mobilization during metamorphism of albitites (circles) and microcline-gneiss (triangle) during metamorphism.

Table 6. Chemical analyses results of major oxides (weight %; total iron expressed as FeO_T) and trace elements Th and Zr (ppm) of amphibolites (samples amp#), albitites (samples alb#), and microcline-gneisses (samples mgn#). CIPW normative mineral contents are also shown.

Sample	SiO_2	TiO_2	Al_2O_3	FeOT	MnO	MgO	CaO	Na_2O	K_2O	P_2O_5	LOI	Total	Zr	Th
Amp2	45.98	2.07	14.66	14.94	0.20	6.15	8.65	4.23	0.81	0.17	0.50	98.36	180	0
Amp4	46.70	2.73	13.99	13.80	0.22	5.65	8.60	3.64	1.92	0.28	0.55	98.08	204	2
Amp1	47.33	2.09	13.77	13.77	0.20	5.89	10.17	2.80	1.35	0.16	0.60	98.13	140	1
Amp5	48.71	2.38	12.94	14.50	0.24	5.31	9.00	2.61	0.32	0.22	2.64	98.87	196	1
Amp6	48.32	1.92	14.63	11.42	0.15	7.29	8.90	4.33	1.54	0.22	0.83	99.55	143	1
Alb18	55.12	0.58	16.19	6.25	0.13	1.22	6.33	8.04	0.64	0.15	5.60	100.25	940	18
Alb2	55.98	0.58	16.26	6.45	0.15	1.90	5.48	7.90	1.03	0.00	5.90	101.63	862	17
Alb1	57.34	0.44	17.13	6.23	0.11	0.77	5.20	8.96	0.46	0.01	4.57	101.22	809	16
Alb8	59.06	0.73	15.24	6.75	0.11	0.57	7.93	7.89	0.20	0.02	0.55	99.05	1389	19
Alb11	59.72	0.55	16.25	5.72	0.14	0.34	7.17	7.65	0.20	0.00	0.31	98.05	990	32
Alb6	61.33	0.47	16.59	6.52	0.11	0.21	6.04	8.35	0.27	0.00	0.39	100.28	982	36
Alb31	62.88	0.58	18.35	5.50	0.03	0.69	2.90	9.11	0.49	0.00	0.26	100.79	1570	21
Alb30	64.49	0.35	17.78	4.65	0.06	0.00	3.01	8.38	0.67	0.00	0.37	99.76	1500	21
Alb23	65.24	0.35	16.79	4.54	0.11	0.18	2.63	9.26	0.24	0.00	0.31	99.65	1590	24
Mgn42	67.40	0.53	14.89	4.34	0.06	0.00	2.15	3.56	5.29	0.00	0.54	98.76	490	7
Mgn23	68.18	0.32	14.63	4.29	0.06	0.27	2.31	3.45	5.25	0.04	0.15	98.95	649	9
Mgn30	68.54	0.32	14.23	5.20	0.07	0.15	1.70	4.03	5.16	0.00	0.20	99.60	555	29
Mgn64	69.60	0.41	13.78	4.90	0.07	0.15	1.96	3.58	5.23	0.00	0.45	100.13	570	14
Mgn52	70.09	0.23	13.79	4.08	0.04	0.00	1.26	4.30	4.38	0.01	0.34	98.52	568	25
Mgn68	72.31	0.24	12.65	3.01	0.05	0.00	1.28	2.62	6.72	0.00	0.87	99.75	474	37
Mgn58	72.50	0.19	13.43	2.65	0.04	0.21	0.85	3.19	6.24	0.00	0.46	99.76	570	80
Mgn62	73.20	0.12	12.46	2.01	0.04	0.00	0.85	2.87	6.20	0.00	0.57	98.32	647	20
Mgn13	73.58	0.22	12.46	2.77	0.02	0.00	0.82	3.02	5.90	0.00	0.34	99.13	516	35

CIPW Norm	Q	Or	Ab	An	Ne	C	Ac	Di Wo	Di En	Di Fs	Hy En	Hy Fs	Ol Fo	Ol Fa	Mt	He	Ilm	Total
amp1	0.00	8.20	19.45	21.55	2.63	0.00	0.00	12.64	5.09	7.67	0.00	0.00	7.02	11.67	0.00	0.00	4.08	100.00
amp2	0.00	4.90	19.30	19.03	9.37	0.00	0.00	10.40	4.08	6.45	0.00	0.00	8.16	14.27	0.00	0.00	4.03	100.00
amp4	0.00	11.68	17.25	16.59	7.80	0.00	0.00	11.40	4.60	6.90	0.00	0.00	6.95	11.52	0.00	0.00	5.33	100.00
amp5	0.00	14.00	20.66	17.04	1.00	0.00	0.00	11.91	4.43	7.71	0.00	0.00	6.38	12.26	0.00	0.00	4.61	100.00
amp6	0.00	9.25	18.74	16.15	9.98	0.00	0.00	11.98	5.90	5.84	0.00	0.00	8.82	9.64	0.00	0.00	3.70	100.00
alb1	0.00	2.82	59.35	5.33	10.30	0.00	0.00	8.92	1.45	8.23	0.00	0.00	0.38	2.35	0.00	0.00	0.87	100.00
alb11	0.53	1.21	66.15	9.61	0.00	0.00	0.00	9.86	0.87	10.07	0.00	0.00	0.00	0.00	0.00	0.00	1.07	99.36
alb18	0.00	4.01	52.93	6.54	10.28	0.00	0.00	11.15	2.62	9.23	0.00	0.00	0.43	1.66	0.00	0.00	1.17	100.00
alb2	0.00	6.36	53.25	6.11	8.94	0.00	0.00	9.31	2.89	6.78	0.00	0.00	1.45	3.76	0.00	0.00	1.15	100.00
alb23	3.11	1.43	78.78	3.55	0.00	0.00	0.00	4.00	0.24	4.24	0.21	3.77	0.00	0.00	0.00	0.00	0.67	100.00
alb30	4.48	3.99	71.26	8.96	0.00	0.00	0.00	2.54	0.00	2.89	0.00	5.22	0.00	0.00	0.00	0.00	0.67	100.00
alb31	0.00	2.88	76.59	7.67	0.00	0.00	0.00	2.77	0.48	2.53	0.01	0.03	0.86	5.08	0.00	0.00	1.10	100.00
alb6	0.00	1.60	67.61	6.98	1.65	0.00	0.00	9.61	0.48	10.31	0.00	0.00	0.04	0.84	0.00	0.00	0.89	100.00
alb8	0.00	1.20	63.34	5.65	2.37	0.00	0.00	11.83	1.45	11.55	0.00	0.00	0.00	0.00	0.00	0.00	1.41	98.80
mgn13	30.13	35.33	25.84	3.01	0.00	0.00	0.00	0.47	0.00	0.53	0.00	4.28	0.00	0.00	0.00	0.00	0.42	100.00
mgn23	20.11	31.44	29.52	8.99	0.00	0.00	0.00	1.09	0.10	1.11	0.58	6.43	0.00	0.00	0.00	0.00	0.62	100.00
mgn30	18.11	30.71	34.27	5.49	0.00	0.00	0.00	1.25	0.06	1.35	0.32	7.84	0.00	0.00	0.00	0.00	0.61	100.00
mgn42	19.30	31.86	30.63	9.14	0.00	0.00	0.00	0.72	0.00	0.82	0.00	6.50	0.00	0.00	0.00	0.00	1.03	100.00
mgn52	23.00	26.39	37.02	5.45	0.00	0.00	0.00	0.38	0.00	0.44	0.00	6.87	0.00	0.00	0.00	0.00	0.45	100.00
mgn58	26.11	37.17	27.15	3.87	0.00	0.00	0.00	0.16	0.02	0.16	0.51	4.50	0.00	0.00	0.00	0.00	0.36	100.00
mgn62	30.35	37.52	24.81	2.82	0.00	0.00	0.00	0.63	0.00	0.71	0.00	2.93	0.00	0.00	0.00	0.00	0.23	100.00
mgn64	21.39	31.03	30.35	6.06	0.00	0.00	0.00	1.55	0.07	1.66	0.30	6.80	0.00	0.00	0.00	0.00	0.78	100.00
mgn68	27.31	40.20	22.39	2.89	0.00	0.00	0.00	1.48	0.00	1.68	0.00	3.59	0.00	0.00	0.00	0.00	0.46	100.00

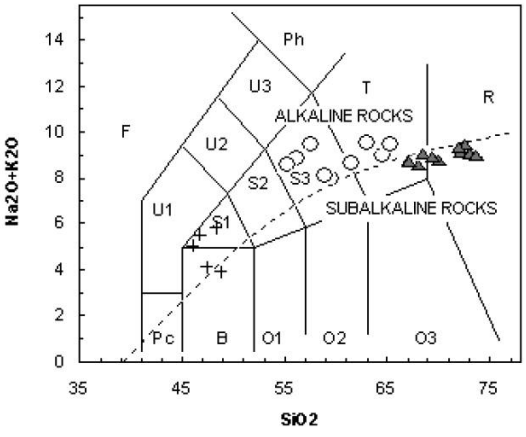

Figure 12. Total alkali-silica – TAS – diagram [37, 40]. Dashed line after [41] separates alkaline and subalkaline rocks. Amphibolite (cross) protolith is a sodic alkali-diorite (S1) and albitite (circle) protolith is a sodic alkaline rock ranging from syenodiorite (S3) to syenite (T). Microcline-gneiss (triangle) protolith is a potassic syenogranite (T and R), however, classified as subalkaline.

formed in sodic syenite, the albitite protolith), Zr, and Th (immobile\incompatible HFS elements) contents. In other words, reasonable trends suggest differentiation of an alkali-dioritic basic magma by fractional crystallization to an intermediate syenitic magma either before or during metamorphism along shear zones. Both alkali-diorite and syenite belong to the same transalkaline series (also named transalkali suite - Figure 12; [39]), which is silica-saturated and characterized by absence of modal nepheline and presence of normative nepheline (see CIPW norm, samples amp# and some alb# - Table 6). Quartz-syenites (non-uraniferous quartz-albitite protolith) are lithostructurally related to uraniferous albitites (see cross-section of the Figure 1) and certainly represent the last magmatic evolutionary step of syenites in the transalkaline series. Although the absence of normative corundum and acmite in syenite and granite allows us to classify them as metaluminous rocks in terms of alumina saturation, Harker diagrams with silica versus major and minor elements reveal trends for Ti, Fe, Mg, Ca and P but Al, Na, K, Zr, and Th (Figures 13 and 14) suggest that there is no petrogenetic relation between albitites (metamorphosed sodic syenites) and microcline-gneiss (metamorphosed granites). Nepheline-normative and sodic transalkaline series (or suite) magmas do not evolve to high quartz-normative subalkaline potassic granitic rocks. Furthermore, abrupt geological contacts in Figure 2 indicate that sodic syenitic magma intruded in previously crystallized potassic granite. This field feature is confirmed by R1 versus R2 diagram [42], after which the geotectonic settings during granitic and syenitic intrusions were syn-collisional and late-orogenic, respectively. In agreement with these settings, U-Pb ages by LA-ICP-MS at 2,009 +/- 78 Ma to microcline-gneiss (older potassic granite) represent syn-collisional episode of the Orosirian Orogeny, and at 1,904 +/- 44 Ma to uraniferous albitites (younger sodic syenite) represent next late-orogenic shearing.

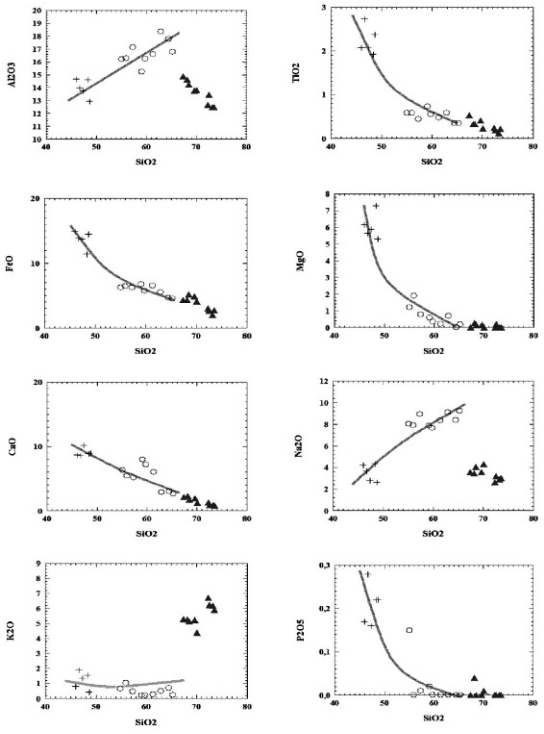

Figure 13. Binary (Harker) diagrams with silica versus major oxides. Cross = amphibolite (protolith = alkali-diorite), circle = uraniferous albitites (protolith = syenitic rocks), triangle = microcline-gneiss (protolith = syenogranite). Curves illustrate the trend between alkali-diorite and syenite.

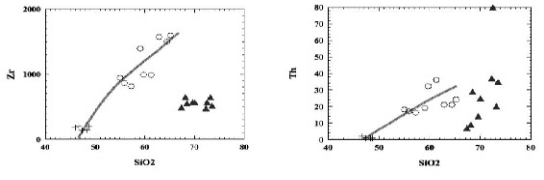

Figure 14. Binary (Harker) diagrams with silica versus trace elements Zr and Th. Cross = amphibolite (protolith = alkali-diorite), circle = uraniferous albitites (protolith = syenitic rocks), triangle = microcline-gneiss (protolith = syenogranite). Curves illustratethe trend between alkali-diorite and syenite.

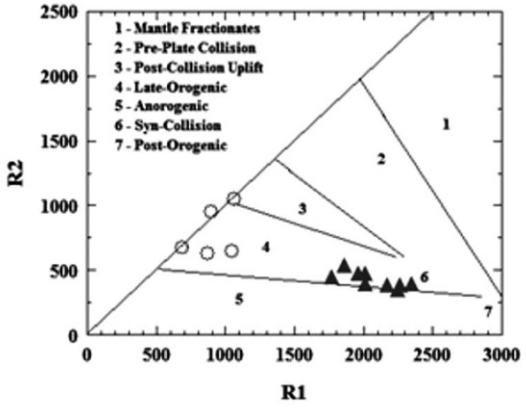

Figure 15. R1 [4Si-11(Na+K)-2(Fe+Ti)] versus R2 [6Ca+2Mg+Al] multicationic diagram [42] of the geotectonic setting discrimination of granitoid rocks, after which syenites (albitite protolith; circles) belong to late-orogenic setting and potassic granites (microcline-gneiss protolith; triangles) belong to syn-collisional setting. Some circles were omitted because they plot outside the field of the diagram.

8. Discussions and conclusions

The initial reason why uraniferous albitites are classified as syenites in this paper and not hydrothermal albitites as previously suggested by [8] and [9] was found during micropetrographic studies, which revealed original magmatic texture (in addition, antiperthites demonstrated more sodic than potassic composition of the feldspars before exsolution). Mixed magmatic and metamorphic textures and frequent exclusively granoblastic texture were generated during shearing. Therefore, the transformation of the magmatic minerals during metamorphism up to complete recrystallization is evident (Figure 3). Besides the recrystallized minerals, new minerals also resulted from the metamorphic reactions. Furthermore, there is no quartz preserved in the U-bearing syenite and features resembling silica dissolution were not found. This contradicts sodic metasomatism of the São Timóteo Granite to generate albitites. Albite, iron-rich augite with melt inclusions, and some microcline are found in parts that preserved the magmatic stage, supporting classification of these rocks as sodic syenites.

In a first high-grade amphibolite facies metamorphic stage not only hastingsite, but also andradite resulting from iron-rich augite transformation appeared (Figure 16A). Simultaneous to the recrystallization of iron-rich augite, albite, microcline (+/- calcite) the accessory minerals formed. During recrystallization, iron-rich augite became more sodic-rich aegirine-augite and albite became slightly more calcic oligoclase. The association between oligoclase and andradite reveals the high pressure metamorphism common to ductile shear zones [27]. Magnetite was replaced by hematite, consistent with oxidizing conditions during metamorphism (e.g. garnet contains only Fe^{3+}).

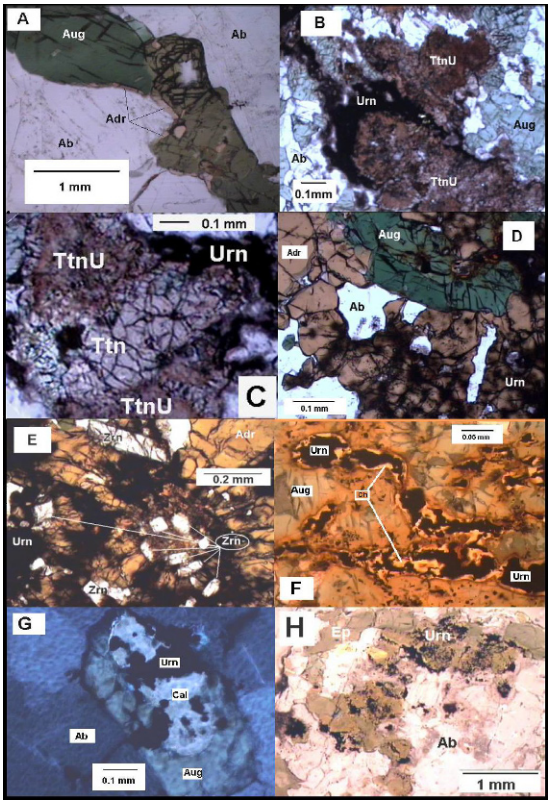

Figure 16. Plate of representative photomicrographs. A: Formation of andradite edge (garnet-Adr) from magmatic iron-rich augite (Aug) in the presence of albite (Ab). B: U-rich magmatic dark brown titanite (TtnU) that released uranium to form uraninite (black - Urn). Augite (Aug) and albite (Ab) also appear in picture. C: U-rich magmatic titanite (TtnU - dark) that released uranium during metamorphism to form uraninite (in black - Urn). Beside it, the recrystallized and fractured uranium-free titanite (Ttn - light) but with uraninite in its fractures also appears. D: Uraninite (in black, metamictic - Urn) inside andradite (Adr - on the left). Aug = augite, Ab = albite. E: Zircon (Zrn – white) and uraninite (in black, metamictic - Urn) inside andradite (Adr). F: Channels (CH) that contain uraninite (in black - Urn) inside recrystallized augite (Aug). Uraninite precipitated in the channels from a solution containing U^{6+} that reacted with the Fe^{2+} of augite. Ab = albite. G: Recrystallized calcite (Cal) with uraninite (Urn) inside augite (Aug; under crossed nichols). Ab = albite. H: Uraninite (black - Urn) inside epidote (Ep).

Uraninite, whose uranium derives essentially from U-rich magmatic titanite (Figure 16B), was also formed during this process. It is usually located near the light coloured recrystallized titanite, inside andradite, hastingsite, and recrystallized augite and calcite (Figure 16C, D and E).

During shearing of U-rich titanite and allanite, aqueous fluids released uranium in the form of U^{+4} and the more mobile oxidized form (uranyl ions – UO_2^{+2}), leading to the formation of uraninite.
The suggested chemical mechanism of the precipitation of uraninite in metamorphosed syenites with or without calcite is described next:
- STEP 1: The U^{4+} ions released from U-rich titanite and allanite during the shear events together with OH^- ions released from the partial hydrolysis of albite, form uraninite in a non-Oxidation/Reduction process

$$U^{4+} + 4\ OH^- \rightarrow UO_2 + 2\ H_2O\ [\text{or } U(OH)_4] \text{ (step 1)}$$

- STEP 2: In metamorphosed syenites without calcite, uraninite interacted completely or partially with the free oxygen circulating through the aqueous fluids during the shearing process. U^{4+} oxidized to aqueous uranyl hydroxide complexes (with U^{6+}), which are stable under temperature and pressure conditions of the shear process [28].

$$2\ UO_2 + 2\ H_2O + O_2 \rightarrow 2\ UO_2^{2+} + 4\ OH^-$$

(step 2 without calcite – Oxidation/Reduction)

In metamorphosed syenites with calcite, calcium carbonate hydrolyzed and formed uranyl tricarbonate complex, which is very stable in the alkaline aqueous environment generated. [29] show that relative abundances of the uranyl tricarbonate complex in solution increase with increasing temperature, under relatively oxidizing and slightly alkaline conditions.

$$2\ UO_2 + 2\ H_2O + O_2 + 6\ CaCO_3 \rightarrow 2[UO_2(CO_3)_3]^{4-} + 4OH^- + 6\ Ca^{2+}$$

(step 2 with calcite – Oxidation/Reduction)

The aqueous alkaline environment certainly facilitated the dissolution of silica from silicates of the rock, and eventually uranyl hydroxisilicate complexes were formed, which also helped in the mobilization of uranium.
Magnetite also interacted with free oxygen and became hematite. The increase in the partial pressure of free oxygen probably favored hematite by the reaction

$$4\ Fe_3O_4 + O_2 \leftrightarrow 6\ Fe_2O_3$$

- STEP 3: Although uranium became extremely mobile in the form of uranyl tricarbonate, the Fe^{2+} of the magmatic augite led to the reduction of U^{6+} to U^{4+} and uraninite to precipitate. The precipitated uraninite was retained inside the recrystallized augite and calcite as well as inside the simultaneously formed andradite. In thin sections, we can clearly notice channels or surfaces containing uraninite, which precipitated when the U^{6+} containing fluid passed through the augite and reacted with its Fe^{2+} (Figure 16F). Uraninite also co-precipitated recrystallized calcite from a uranyl-tricarbonate containing fluid, after reaction with Fe^{+2} of the augite (Figure 16G):

$$3\ Ca^{2+} + [UO_2(CO_3)_3]^{4-} + 2\ Fe^{2+} \rightarrow UO_2 + 2\ Fe^{3+} + 3CaCO_3$$

(step 3 with calcite – Oxidation/Reduction)

In metamorphosed syenites without calcite, the following reaction is suggested for precipitation of uraninite:

$$UO_2^{2+} + 2\ Fe^{2+} \rightarrow UO_2 + 2\ Fe^{3+} \text{ (step 3 without calcite – Oxidation/Reduction)}$$

Similar Oxidation/Reduction processes have already been experimentally described by [30] for hydrothermal conditions. [9] previously suggested that uraninite precipitation in Lagoa Real was controlled by the reduction of an uraniferous fluid phase, via progressive oxidation of mafic minerals.
Epidote and biotite appeared during a new metamorphic stage. They partially replaced the minerals formed during the initial metamorphism. This paragenesis indicates a re-equilibrium established under new temperature and pressure conditions, less intense than the ones which formed garnet during the initial metamorphism. It is interesting to note that uraninite crystals are also found inside epidote (Figure 16H) and biotite suggesting a similar precipitation reaction as that described in steps 2 and 3. Biotite contains both Fe^{2+} and Fe^{3+} while in epidote only Fe^{3+} occurs. Uraninite precipitation inside these minerals, eventually with involvement of calcite, would have occurred under these new metamorphic conditions, between greenschist and amphibolite facies.
The generation of magmas in subduction zones is thought to be the most important mechanism to the growth of continental crust since the Proterozoic. Most of these magmas derive from the melting of the mantle wedge above the subducted slab driven by its dehydration. The interaction between fluids generated during this dehydration and overlaying mantle material would be responsible for the trace and rare earth elements, thorium, and uranium enrichment in magmas [16]. During the late Orosirian orogenic stages, ductile shear fault zones probably controlled the site of emplacement of alkali-diorite and syenite studied here. The Lagoa Real syenites certainly have formed by crystal fractionation of ferromagnesian silicates and calcic plagioclase from dioritic parent magmas, currently represented by closely associated local amphibolites. Therefore, the syenitic rocks have lower abundances of Ca, Mg and Fe than diorites, but generally

higher abundances of Na, which is supported by the predominant occurrence of sodic plagioclase together with augite. This explanation differs from the sodic metasomatism proposed by [8, 9] and [12] generating an age of attaining 1,750 Ma for the São Timóteo Granite. According to [8, 9] and [12], augites from metamorphosed syenites (uraniferous albitites) would have derived from the dehydration of amphiboles during metamorphism of the 1,750 Ma São Timóteo Granite. According to this study, however, augites are of magmatic origin around 1,900 Ma ago.

Melt inclusions found in magmatic augite are richer in Na, Al and Ti than the augite host. These elements belonged to the magma when augite crystallized and were further incorporated by albite (Na and Al) and uraniferous titanite (Ti) during syenite crystallization processes. There is some radiogenic Pb in the augite structure, which reveals the presence of U in the syenite magma. Primary fluid inclusions in magmatic iron-rich augite of the albitite suggest a sodium-rich original magma, making sodic metasomatism obsolete. Therefore, a magmatic model for the Lagoa Real uraniferous albitites is reasonable; however, metasomatic alteration of microcline gneiss cannot be totally excluded: The sharp contacts in Fig. 2 might be caused by fluid infiltration. Trends between SiO_2 and major and minor elements are partly contradictory and age data of these two rock types overlap within error range.

Accessory minerals like zircon, titanite, allanite, and apatite accompany uraniferous syenites. They preferentially incorporate U, Th and rare earth elements, incompatible to the structure of the major silicates in these rocks. Due to the resemblance of the ionic potentials of U and Ti, titanite is the most probable primary uranium-bearing mineral (figures 16B and C). Uranium was released during the metamorphic episodes to form uraninite in an almost closed system. In this way, the data of the present work deviate from the model suggested by [8]. [8] proposed that desilicification and uranium-rich fluids derived from accessory minerals of the quartz-rich São Timóteo Granite generated the uraniferous albitites by metasomatic processes.

Parts of the genetic model of the Uraniferous Province proposed by [4], which associates uranium to "polycyclic diapiric processes", is in agreement with the present work. However, according to this author, the diapirism occurred during the Brasiliano event, which does not concur with the Orosirian geochronological data of the magmatism described here.

[14] pointed out that many important uraniferous provinces in the world are ultimately related to evolved felsic igneous rocks intruded at shallow levels of the crust, either anorogenically or during the final stages of orogenesis. The present investigations suggest that uranium from Lagoa Real albitites is related to the syenitic magmatism belonging to mafic/felsic association linked to the final stages of the Orosirian Orogeny in the Paramirim Block around 1,900 Ma. The ductile shearing that affected? the uraniferous syenites (albitites) formed uraninite in these rocks not only during the Orosirian metamorphism, when these rocks became metasyenites due to intense recrystallization of its minerals, but also in the later Brasiliano metamorphism.

There are two geotectonic implications resulting from the present study. The first one is the confirmation of the Orosirian orogenetic event in the Paramirim Block that culminated in the tectonic structuring of the São Francisco/Congo Craton in the Palaeoproterozoic, probably through collision between West São Francisco and East São Francisco/Congo continental masses. The N-S trending sutures in Paramirim Block, visible in the Geologic Map of Bahia [43], were presumably reactivated from the Palaeoproterozoic orogeny after the Orosirian event. The second implication is the confirmation of the Brasiliano event in the region as proposed by [21] and [12]. The reactivation of Orosirian shear zones and metamorphism in Paramirim Block during Proterozoic/Phanerozoic transition would have been promoted by continental aggregation processes, which led to the appearance of West Gondwana.

According to the lithogeochemical data the magmatic composition can be recognized in all studied samples. This observation implies surprisingly isochemical processes during the metamorphism, which created the Lagoa Real albitites. This is quite different from the previous metasomatic models. The data point towards a petrogenetic association between alkali-diorite (amphibolite protolith) and sodic syenite (albitite protolith) by fractional crystallization through transalkaline series developed in a Palaeoproterozoic late-orogenic tectonic scenario. This magmatic differentiation occurred either before or during shearing, which in turn led to the albitite and amphibolite formation. The microcline-gneiss, whose protolith is a syn-collisional potassic granite, represents the albitite host rock and is apparently not petrogenetically associated to the late-orogenic sodic syenite (albitite protolith).

A review study of mafic and felsic magmas in within-plate regimes worlwide [44] identified not only that late- to post-orogenic igneous associations yielded less potassic and more sodic compositions, but also that the igneous suites, comprising mafic and felsic rocks, range from alkali-calcic metaluminous to alkaline, which are precisely the characteristics of the Lagoa Real alkali-diorite (amphibolite protolith) and sodic syenite (albitite protolith). Furthermore, [44] proposed that such igneous associations evolve

progressively into more markedly alkaline within-plate suites, suggesting that the 1.75 Ga anorogenic alkaline São Timóteo Granite represents the closing within-plate stage of the aforementioned tectonic scenario.

Acknowledgments

Thanks go to CNPq for the author's Post-Doctoral research support, to the Development Center of Nuclear Technology (CDTN-CNEN), to the Memorial University of Newfoundland (Canada), where geochronological studies by LA-ICP-MS were carried out, and to the Brazilian Nuclear Industries (INB) for field work and sampling support.

References

[1] Costa P.H.O., Andrade A.R.F., Lopes G.A., Souza S.L.. Projeto Lagoa Real: Mapeamento Geológico, 1:25.000. Salvador: CBPM, 1985

[2] CPRM. Catálogo geral de produtos e serviços. Geologia. Levantamentos Aerogeofísicos. Base de dados Aerogeofísicos, Rio de Janeiro, Geologia e Recursos Hídricos, 1995

[3] Garrido I.A.A., Silva R.W.S., Mascarenhas J.F., Interpretação integrada de dados magnéticos e gamaespectrométricos – Área Ibitiara-Rio das Contas, Bahia Brasil [Integrated interpretation of gammaspectrometric and magnetic data - Ibitiara-Rio das Contas Area, Bahia - Brazil]. Programa de Levantamentos Aerogeofísicos – CBPM. 2002

[4] Geisel Sobrinho E., Apresentação de uma hipótese genética para o Distrito Uranífero de Lagoa Real [Presentation of a genetic hypothesis for the Uraniferous District of Lagoa Real]. Nota Técnica EBHO.PM No. 3, Nuclebrás, 1981

[5] Alves J.V., Fuzikawa K., O estudo de inclusões fluidas da jazida uranífera de Cachoeira-Caetité, BA: resultados preliminares [The study of fluid inclusions of the Cachoeira Uraniferous deposit - CaetitÃť, BA:preliminary results]. In: Anais do Congresso Brasileiro de Geologia, 33, Rio de Janeiro. Sociedade Brasileira de Geologia, V.3, 1984, 1503-1517.

[6] Oliveira A.G., Fuzikawa K., Moura L.A.M., Raposo C., Província uranífera de Lagoa Real – BA [Lagoa Real Uraniferous Province], *Principais Depósitos Minerais do Brasil* – DNPM (National Department of Mineral Production) 5, 1985, 105-120.

[7] Turpin L., Maruejol P., Cuney M., U-Pb, Rb-Sr and Sm-Nd chronology of granitic basement, hydrothermal albitites and uranium mineralization (Lagoa Real, South-Bahia, Brazil). *Contributions to Mineralogy and Petrology*, 98, 1988,139-147

[8] Maruejol P., Métasomatose alcaline et minéralisations uranifčres: les albitites du gisement de Lagoa Real (Bahia, Brésil) et exemples complémentaires de Xihuashan (SE Chine), Zheltorechensk (Ukraine) et Chhuling Khola (Népal central) [Alkaline metasomatism and uraniferous mineralization: albitites of the Lagoa Real (Bahia, Brazil) and additional examples Xihuashan (SE China) Zheltorechensk (Ukraine) and Chhuling Khola (Central Nepal)]. These Docteur. - Centre de Recherches sur la Géologie de l'Uranium, Nancy, France, 1989

[9] Lobato L.M., Fyfe W.S., Metamorphism, Metasomatism, and Mineralization at Lagoa Real, Bahia, Brazil. *Economic Geology*, 85, 1990, 968-989

[10] Pimentel M.M., Machado N., Lobato L.M., Geocronologia U-Pb de rochas graníticas e gnáissicas da região de Lagoa Real (BA) e implicações para a idade da mineralização de Urânio [U-Pb geochronology of granitic and gneissic rocks of the Lagoa Real (BA) region and implications for the age of uranium mineralization]. Anais do XXXVIII Congresso Brasileiro de Geologia, Camboriú, 1994, 389-390

[11] Pascolathi E.M., Silva C.L., Costa S.S., Osako L.S., Amaral G., Rodriguez I.P., Novas ocorrençias de urânio na região de Lagoa Real, a partir da superposição de dados geofísicos, geológicos e de sensoriamento remoto [New occurrences of uranium in the region of Lagoa Real from the superimposition of geophysical, geological and remote sensing data]. *Revista Brasileira Geociençias*, 33, 2003, 91-98

[12] Cruz S.C.P., A interação entre o Aulacógeno do Paramirim e o Orógeno Araçuaí-Oeste Congo [The interaction between Paramirim aulacogen and the Araçuaí-West Congo Orogen]. Tese Doutorado-UFOP, Contribuições ís Ciençia da Terra – Série D, 2004

[13] Cordani U.G., Iyer S.S., Taylor K., Kawashita K., Sato K., McReath I., Pb-Pb, Rb-Sr, and K-Ar systematics of the Lagoa Real uranium province (south-central Bahia, Brazil) and the Espinhaço Cycle (ca. 1.5-1.0 Ga). *Journal of South American Earth Sciences*, 5, 1992, 33-46

[14] Plant J.A., Simpson P.R., Smith B., Windley B., Uranium ore deposits – products of the radioactive Earth. In: Burns, P.C. and Finch, R. (Eds.) - Uranium: Mineralogy, Geochemistry and the Environment. *Reviews in Mineralogy*, 33, 1999, 255-307

[15] Bonin B., From orogenic to anorogenic magmatism:

a petrological model for the transition calc-alkaline – alkaline complexes. *Revista Brasileira Geociençcias*, 17, 1987, 366-371

[16] Keppler H., Constraints from partitioning experiments on the composition of subduction-zone fluids. *Nature*, 380, 1996, 237-240

[17] Inda H.V.A., Barbosa J.S.F., Texto explicativo para o mapa geológico do Estado da Bahia (1:1.000.000). In: J.S.L. Barbosa, Dominguez J.M.S., Geologia da Bahia (texto explicativo). Salvador, Secretaria da Industria, Comércio e Mineração, Superintendęncia de Geologia e Recursos Minerais, 1996

[18] Mascarenhas J.F., A geologia do centro-leste do Estado da Bahia [The geology of central-east of the Bahia State]. In: Anais do XXVII Congresso Brasileiro de Geologia, Aracaju, 1973, 2, 35-66

[19] Almeida F.F., O Cráton do São Francisco. *Revista Brasileira Geociençcias*, 7, 1977, 349-364

[20] Cordani U.G., Brito Neves B.B., The geologic evolution of South America during the Archaean and Early Proterozoic. *Revista Brasileira Geociençcias*, 12, 1982, 78-88

[21] Caby R., Arthaud M., Petrostructural evolution of the Lagoa Real subalkaline metaplutonic complex (Bahia, Brazil). *Revista Brasileira Geociençcias*, 17, 1987, 636

[22] Ribeiro C. I., Carvalho Filho C. A., Hashizume S., As jazidas de urânio de Lagoa Real [The uranium deposits of Lagoa Real]. Anais do XXXIII Congresso Brasileiro de Geologia, 1984, 1463-1474

[23] Sylvester P., Laser Ablation-ICP-MS – Principles and Applications. Short Courses Series, 29, Mineralogical Association of Canada, 2001

[24] Stacey J.S., Kramers J.D., Approximation of terrestrial lead isotope evolution by a two-stage model. *Earth and Planetary Science Letters*, 26, 1975, 207-221

[25] Ludwig K.R., Isoplot/Ex 3.00: A geochronological toolkit for Microsoft Excel. Berkeley Geochronology Center, Special Publication, 2003, 4

[26] Gregory M.J., Wilde A.R., Jones P., Uranium deposits of the Mount Isa region and their relationship to deformation, metamorphism and Cu deposition. *Economic Geology*, 100, 2005, 537-546

[27] Yardley B.W.D., Introdução ŕ Petrologia Metamórfica. EDUNB (translated edition). 1989

[28] Finch R., Murakami T., Systematics and Paragenesis of uranium minerals. In: Burns P.C., Finch R.J. (Eds), Uranium: Mineralogy, Geochemistry and the Environment. *Reviews in Mineralogy*. Mineralogical Society of America, 38, 1999, 91-166

[29] Kojima S., Takeda S., Kogita S., Chemical factors controlling the solubility of uraninite and their significance in the genesis of unconformity-related uranium deposits. *Mineralium Deposita*, 29, 1994, 353-360

[30] Rafalskii R.P., Kudunova K.F., Experimental investigation of the conditions of the reduction and precipitation of uranium by minerals. *Atomic Ene*rgy, 1961, 7, 815-818.

[31] Pickhardt C., Dietze HJ., Becker J.S., Laser Ablation Inductively Coupled Plasma Mass Spectrometry for direct isotope ratio measurements on solid samples. *International Journal of Mass Spectrometry*, 242, 2005, 273-280

[32] Guimarães J.T., Teixeira L.R., Silva M.G., Martins A.A.M, Filho E.L.A., Loureiro H.S.C., Arcanjo J.B., Dalton de Souza J., Neves J.P., Mascarenhas J.F., Melo R.C., Bento R.V., Datações U-Pb em rochas magmáticas intrusivas no Complexo Paramirim e no Rifte Espinhaço: uma contribuição ao estudo da evolução geocronológica da Chapada Diamantina [U-Pb dating on magmatic intrusive rocks of the Paramirim complex and Espinhaço rift: a contribution to the study of the geochronological evolution of the Chapada Diamantina]. In: Anais do III Simpósio do Cráton São Francisco. Salvador, Bahia, 2005

[33] Alkmin F.F., Marshak S., Transamazonian orogeny in the southern São Francisco Craton region (MG), Brazil: Evidence for Palaeoproterozoic collision and collapse in the Quadrilátero Ferrífero. *Precambrian Research*, 90, 1998, 29–58

[34] Heinrich C.A., Pettke T., Halter W.E., Aigner-Torres M., Audetat A., Gunther D., Hattendorf B., Bleiner D., Guillong M., Horn I., Quantitative multi-element analysis of minerals, fluid and melt inclusions by Laser Ablation Inductively Coupled Plasma Mass Spectrometry. *Geochimica Cosmochimica Acta*, 67, 2003, 3473-3496

[35] Richard L.R.. Minpet version 2.02 - Mineralogical and petrological data processing system for Windows., Quebec – Canada, 1996

[36] Pearce T.H., A contribution to the theory of variation diagrams. *Contributions to Mineralogy and Petrolology*, 19, 1968, 142-157

[37] Le Bas M.J., Le Maitre R.W., Streckeisen A. Zanettin B., A chemical classification of volcanic rocks based on the total alkali – silica diagram. *Journal of Petrology*, 27, 1986, 745–750

[38] Whitney D.L., Evans B.W., Abbreviations for names of rock-forming minerals. *American Mineralogist*, 95, 2009, 185-187

[39] Middlemost E.A.K., Towards a comprehensive classification of igneous rocks and magmas. *Earth Science Reviews*, 31, 1991, 73-87

[40] Le Maitre R.W., Igneous Rocks - A classification and Glossary of Terms. Recommendations of the Interna-

tional Union of Geological Sciences, Subcommission of the Systematics of Igneous Rocks. Cambridge University Press, Cambridge, 2002

[41] Irvine T. N., Baragar W.R.A., A guide to the chemical classification of the common volcanic rocks. *Canadian Journal Earth Sciences*, 8, 1971, 523-548

[42] Batchelor R. A., Bowden P., Petrogenetic interpretation of granitoid rock series using multicationic parameters. *Chemical Geology*, 48, 1985, 43-65

[43] CPRM/CBPM. Geologia e Recursos Minerais do Estado da Bahia – Sistema de Informações Geográficas, 2003, CD-ROM

[44] Bonin B. Do coeval mafic and felsic magmas in post-collisional to within-plate regimes necessarily imply two contrasting, mantle and crustal, sources? A review. *Lithos*, 78, 2004, 1-24

[45] Deer W.A., Howie R.A., Zussman J., An introduction to the rock forming minerals. Longman Group Ltd., London, 1966

[46] Hawthorne F.C, Oberti R., On the classification of amphiboles. *Canadian Mineralogist*, 44, 2006, 1-21

[47] Nesbitt H.W., Young G.M., Early Proterozoic climates and plate motions inferred from major element chemistry of lutites. *Nature*, 299, 1982, 715-717

[48] Garcia L.R.A., Introdução ŕ Microscopia Eletrônica de Varredura e ŕ Microanálise. Centro de Desenvolvimento da Tecnologia Nuclear – CDTN [Introduction to Scanning Electron Microscopy and Microanalysis]. Belo Horizonte, 2001